Design and Experimental Validation of Reorientation Manoeuvres for a Free Falling Robot Inspired from the Cat Righting Reflex

Xavier Garant and Clément Gosselin, *Fellow, IEEE*

***Abstract*—This paper presents two distinct manoeuvres allowing an articulated robot in free fall to change its orientation using closed paths in the joint space. It is shown through dynamics simulations that the magnitude of the net rotation is dependent upon the amplitude of the angular displacement of the joints. With realistic joint limitations, the robot, which includes rotary actuators only, can perform a 180-degree reorientation about its longitudinal axis, similar to the cat righting reflex. The second manoeuvre allows the robot to accomplish rotations of smaller magnitude about a different axis. A physical prototype and a VICON motion tracking system are used to experimentally validate the simulation results. Finally, it is shown that the two manoeuvres, which yield rotations about fixed axes, can be repeated and alternated to enable the robot to reach any arbitrary 3D orientation.**

***Index Terms*—Nonholonomic mechanisms and systems, dynamics, biologically-inspired robots, underactuated robots.**

I. Introduction

THE elusive phenomenon of the self-righting cat falls under the category of problems governed by the law of constant angular momentum. Indeed, with nothing to push against, the cat manages to modify its orientation while free falling, by using the movements of its spine and limbs exclusively. Kane and Scher [1] were among the first to prove that a simplified mathematical model-cat could accomplish a 180 degree flip by executing a specific sequence of movements of the spine. Naturally, several research initiatives in the field of robotics sprouted from the study of this particular phenomenon, and the more general case of reorienting a mechanical system of articulated bodies [2]. As a matter of fact, it is nowadays possible to consider applications where having this ability is not only relevant but essential for a robot. Notably, posture control while falling to mitigate impact for articulated robots was investigated in [3], [4]. Lizard-like self-righting through the use of a tail was studied with simplified systems composed of two bodies in [5], [6], [7]. More recently, there has been a growing interest towards more complex terrestrial mobile robots such as bio-inspired legged robots. One relevant example is the MIT Mini Cheetah, which can perform a backflip by using an offline nonlinear optimisation technique [8]. This quadruped robot is also intended to be able to regulate its body orientation in mid-air in the future, to compensate for varying starting and landing conditions.

Another problem which is closely related to the falling cat phenomenon is the reorientation of humans in free fall. Gymnasts and divers are frequently confronted to this situation as they perform twists and flips in mid-air with zero initial angular momentum [9], [10]. Moreover, with the advent of human spaceflight, these manoeuvres were studied extensively [11], [12], [13], [14] in order to devise ways for astronauts to change their orientation in weightlessness. However, most of the theoretical research in this area is centred on space systems and satellite control. The ability to control the orientation of multi-body space systems using internal movements could notably reduce the amount of propellant needed and save weight by removing the need for auxiliary systems such as reaction wheels or magnetic torquers. Several modelling methods have been proposed for free-floating space manipulators, like the virtual manipulator approach [15] and the generalised Jacobian [16]. Nonlinear control models based on Lie brackets and controllability for this case of nonholonomic problem have also been investigated in depth [17], [18], [19], [20].

One more potential application for free fall reorientation lies at the intersection of space systems and terrestrial robot research – the robotic exploration of celestial bodies. Already, the use of hopping as a means of locomotion in this context has been the scope of many research and development initiatives. Notable examples include the DLR compliantly actuated quadruped, whose long term application is autonomous plane-

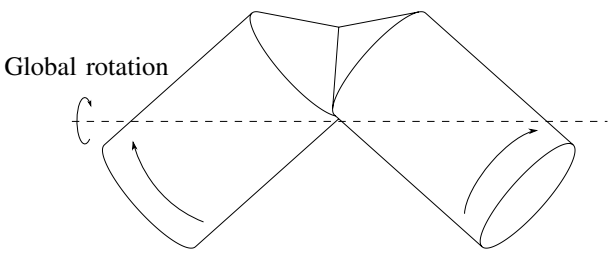

Fig. 1. Cat reorientation model : a free-floating system of two bodies rolling on their conical ends. Momentum conservation dictates that the system rotate as a whole in this situation.

This work was supported by the Natural Sciences and Engineering Research Council of Canada (NSERC) and the Canada Research Chair program. *(Corresponding author: Xavier Garant.)*

The authors are with the Department of Mechanical Engineering, Université Laval, Québec, QC G1V 0A6, Canada (e-mail: xavier.garant.1@ulaval.ca, gosselin@gmc.ulaval.ca).

This paper has supplementary downloadable material available at http://ieeexplore.ieee.org, provided by the authors.

Colour versions of one or more of the figures in this paper are available online at http://ieeexplore.ieee.org.

tary exploration [21] and the SpaceBok legged robot, which is designed for extended flight phases [22]. Thus, having some form of attitude control during the jump phases is arguably even more critical for this kind of robot [23], compared to terrestrial robots such as the MIT Mini Cheetah.

While reproducing weightlessness conditions in 3D space on Earth remains a challenge, several research initiatives have resulted in interesting experimental work. For instance, the results in [24], [25], [26] show that a tailed robot can effectively accomplish inertial reorientation in at least one plane. The in-depth analysis of [27] and the simulations in [28] concluded that the use of a tail or appendages is particularly interesting for terrestrial robots and also explored the use of flailing limbs. However, although such inertial devices can be effectively integrated in some robot designs, it might not always be possible or desirable to add dedicated appendages such as multiple-degree-of-freedom (DOF) tails or joints with an infinite range of motion. Moreover, in some cases, these methods take advantage of the fact that the joint trajectories do not form closed paths, i.e., the robot's landing configuration differs from its starting configuration.

In a previous paper, a planar robot that relied on closed-loop movements for reorientation was proposed [29]. However, the planar architecture of the robot still required it to collide with itself to accomplish significant rotations. In practice, robotic manipulators indeed have joint limits to prevent self-collision. One example of a practical robot capable of righting itself in free fall while incorporating joint limitations is presented in [30]. This robot, which is based on Kane and Scher's model, uses a Lie bracket control to generate the desired reorientation, without using appendages. This type of model was also experimentally validated in [31]. Finally, the effect of the angle of the distal links during a cat-like reorientation was investigated with a practical robot in [32]. The same model was also used in [33] to demonstrate by simulations that these distal links can be used to fine-tune the pitch orientation of the robot, in order to obtain a desired landing posture.

Free-floating systems are often bound to be inherently hyper-redundant. Indeed, their primary task, such as walking or manipulation, in the case of terrestrial and space robots respectively, generally involves a high number of actuated DOFs, while spatial reorientation is a three-dimensional task. This article seeks to simplify this complex reorientation problem by decomposing it into simple and well-known movements, as a step towards motion primitive path planning. To this end, it is proposed to reduce the system to a simpler set of subsystems and draw from the literature pertaining to the cat righting reflex. Thus, two manoeuvres for reorienting an articulated robot under zero angular momentum in a weightless environment are proposed. Much like the cat motion itself, the method relies on closed paths (loops) in the joint space to produce a net change in orientation. Practically, this means that the change in orientation is not specifically imparted to an end-effector or certain links, but to the robot as a whole. In summary, this paper notably contributes to the current literature in the following respects. By showing a way to effectively reduce a hyper-redundant robot to a simpler "self-righting cat" model, two simple reorientation manoeuvres can be introduced. Each of these manoeuvres results in a distinct reorientation and one is particularly effective at "flipping" a robot. Both manoeuvres are applicable to various robot architectures as long as they can be reduced to the simpler model. The practical feasibility and general behaviour of these manoeuvres with regards to typical design parameters are investigated. Another main contribution is the demonstration that the two manoeuvres are sufficient to reach any orientation. Finally, this article also proposes a rigorous non-trivial experimental validation method based on quantitative motion tracking data.

This paper is structured as follows. Section II reviews a cat reorientation model and provides insight on the inspiration for the manoeuvres presented in the paper. The proposed reorientation manoeuvres are then described in Section III. The mathematical model, which is based on the conservation of angular momentum, is introduced in Section IV. Section V presents the design of the prototype of an articulated robot on which the proposed manoeuvres are implemented. Simulation results obtained with a dynamic simulation program are then presented in Section VI, where the effects of some of the design parameters on the reorientation are studied and discussed. Section VII discusses how combining the two manoeuvres enables the robot to reach any arbitrary orientation. Section VIII presents the experimental validation of the manoeuvres using the physical 3-DOF articulated prototype. Finally, conclusions are drawn in Section IX.

II. Basic Model and Inspiration

Of the many representations of the cat righting reflex, a visual and intuitive one can be obtained by considering two bodies with a conical surface at one end [9]. One can consider these as the upper and lower parts of the body of a cat. As shown in Fig. 1, if the two conical surfaces are allowed to roll on each other without slipping when the bodies rotate about their own axis, then the whole system will experience a rotation about a horizontal axis. This is a consequence of the conservation of momentum, as the system must rotate to compensate for the rotation of the bodies, in order to maintain zero total angular momentum.

Interestingly, another conclusion can be drawn from the same model. By relaxing the no-slip constraint and assuming that the bodies rotate in the same direction (instead of opposite), we find that the global system must rotate about a vertical axis to conserve momentum. This is not typical of cats, but nevertheless has relevant implications. Indeed, for an identical initial configuration, a simple reversal of the direction of rotation of one body yields a completely different reorientation of the system.

While this model has relevant theoretical value, its practicality is limited in the context of robotic applications. First, this architecture serves a single purpose, which is reorienting in free fall, meaning it is not versatile. Second and more importantly, reorienting using this architecture does not allow for closed loops in the configuration space, i.e., the initial and final joint values are not equal. In practice, robots have a limited range of joint motion, and reaching a desired orientation at the end of this range is virtually useless in many situations, since the robot cannot move further.

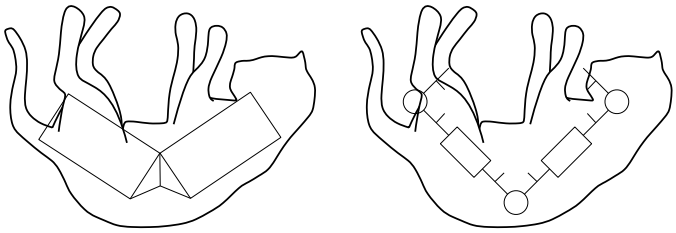

Fig. 2. Cat model analogy : Rolling cone model (left). Proposed articulated robot (right).

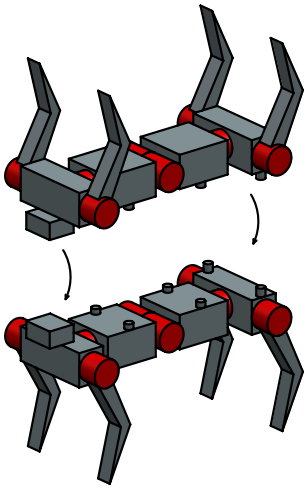

Fig. 3. The proposed articulated robot model can be pictured as a simplified quadruped robot. The joints are shown in red.

Thus, this work focuses on a more general articulated robot model. The model (shown on the right-hand side of Fig. 2) is general in the sense that it is solely comprised of generic links connected in series by revolute joints of alternated directions. The three central revolute joints, with intersecting axes, can be thought of as a generalised implementation of the rolling cones, where the cone angle can be modified using the central joint. This architecture is analogous to the common 7-DOF shoulder-elbow-wrist serial manipulator architecture, leaving out one joint at each end. One can also picture this model as a representation of a legged robot which can twist its spine, or has the ability to rotate its upper and lower body (Fig. 3). With this model, it is possible to carefully devise sequences of movements which mimic the rolling cone cat model, while allowing the robot to return to its initial configuration in joint space. This net global reorientation through closed-loop joint trajectories is made possible by varying the moments of inertia of the robot between each joint actuation, as detailed in the following section.

III. Reorientation Manoeuvres

The first proposed manoeuvre (referred to as manoeuvre A) can be decomposed in 6 steps, as shown in Fig. 4. Transposing this method to the falling cat would imply that the animal twists its body along the spine axis, as opposed to Kane and Scher's "no-twist" model [1], [24], [25], [30], [31]. There are

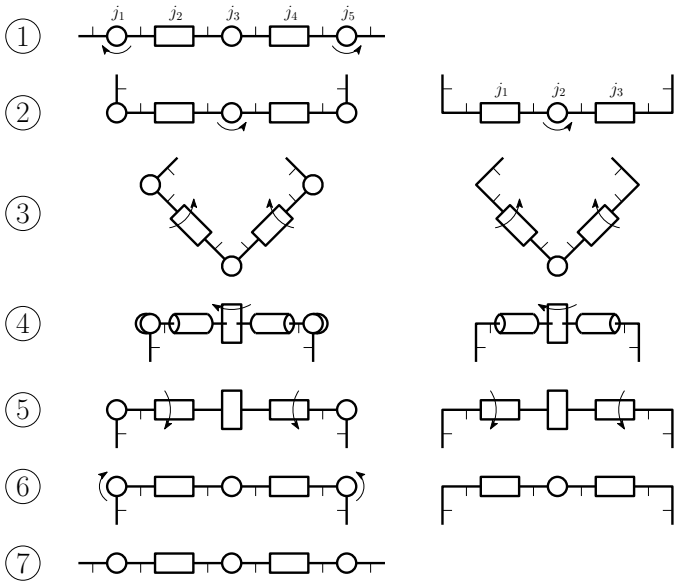

Fig. 4. Description of manoeuvre A: Manoeuvre steps for a six-body, five-joint architecture (left). Manoeuvre steps for a four-body, three-joint architecture (right). The robot is shown at each step in its configuration before beginning the indicated rotation. Thinner line stubs show link orientation. Joints j_i are numbered from left to right.

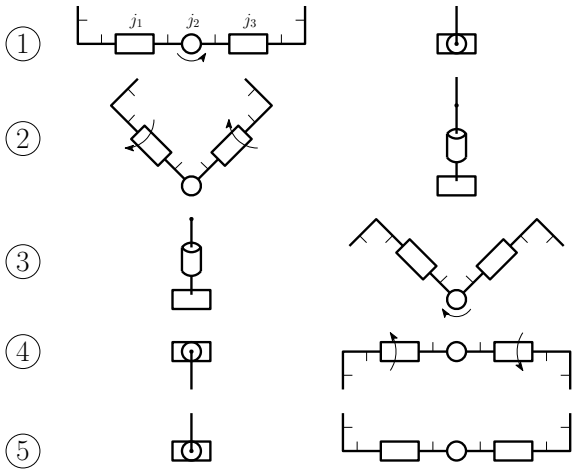

Fig. 5. Description of manoeuvre B: Front view, manoeuvre steps for a four-body, three-joint architecture (left). Side view, manoeuvre steps for a four-body, three-joint architecture (right). The robot is shown at each step in its configuration before beginning the indicated rotation. Thinner line stubs show link orientation. Joints j_i are numbered from left to right.

diverging opinions on whether the cat effectively does so [9]. However, the manoeuvre is also comparable to a "swivel-hips" that trampolinists execute to rotate their body 180 degrees [9].

The manoeuvre is well suited for a serial articulated robot composed of six bodies and five rotary actuators. In addition, this architecture does not rely on an actuated Hooke joint, in contrast with other works in the literature that use the "no-twist" model. The system can also be reduced to four bodies and three rotary actuators for simplicity, without notable loss of performance. We can discard steps 1 and 6 and use an "L" shape for the first and last links of the chain, without actuators 1 and 5, as shown in Fig. 4. This simplifies the experimental process by reducing the number of control inputs and allowing

more time for the most important parts of the sequence before the robot touches the ground.

The manoeuvre works by changing the moment of inertia of certain parts of the system between each actuation of the joints. For instance, at step 3, when actuating joint 2 of the six-body system, the moment of inertia (with respect to the joint axis) of the combined bodies to the right of the joint is much larger than the moment of inertia of the bodies to the left. Thus, qualitatively, the left segment will be subject to a large rotation, while the right segment will experience little rotation. By contrast, at step 5, the relative moments of inertia of the left and right sides are similar, therefore both sides will rotate by a similar amount. This way, the relative angle between each link always returns to its original value at the end of the manoeuvre, effectively meaning that the robot goes back to its starting configuration in the joint space.

A very different reorientation can be obtained by a slight variation of the sequence, while keeping the same robot architecture. As shown in Fig. 5, by reversing the direction of rotation of joint 1 or joint 3 of the four-body system, the robot performs what can be compared to a "signal flag" motion [11] (referred to as manoeuvre B). Concretely, this allows for net rotations mainly about the yaw axis of the robot, while manoeuvre A allows for net rotations about the roll axis.

Manoeuvres such as those presented above, when executed in free fall, have the interesting characteristic of being time-independent. In other words, the speed at which the manoeuvre is executed has no impact on the final state of the system: only the geometric path in the joint space matters. A mathematical proof of this property can be found in [34]. Thus, we can use a representation of the paths in joint space without losing significant information, and use this to our advantage for easier parametrisation of the trajectories. The proposed manoeuvres for the simplified three-joint architecture are therefore represented as a closed path in the joint space.

IV. Mathematical Background

In order to provide a better understanding of the physics at play during the reorientation, the dynamic model of a free-floating serial robot with n links and j revolute joints ($j = n-1$) is derived in this section. The formulation presented here was proposed in [29] as an adaptation of [15]. This model assumes that the multibody system is free-floating and initially at rest.

Free-floating manipulators differ from their earth-based counterparts in that the position and orientation of each link depend on the position and orientation of every other link in the chain [35]. As a consequence of the conservation of momentum, the dynamic behaviour of a free-floating multibody system can be expressed with respect to its global centre of mass (CM), as shown in Fig. 6. Since the position of the CM is constant in any reference frame (in this case R_0) moving with the robot, the position $\mathbf{r}_i$ and velocity $\mathbf{v}_i$ of the centre of mass (CM_i) of link $i\,(i = 1, \ldots, n)$ is related to that of the other bodies as follows

$$\sum_{i=1}^{n} m_i \mathbf{r}_i = \mathbf{0}\,, \quad \sum_{i=1}^{n} m_i \mathbf{v}_i = \mathbf{0} \tag{1}$$

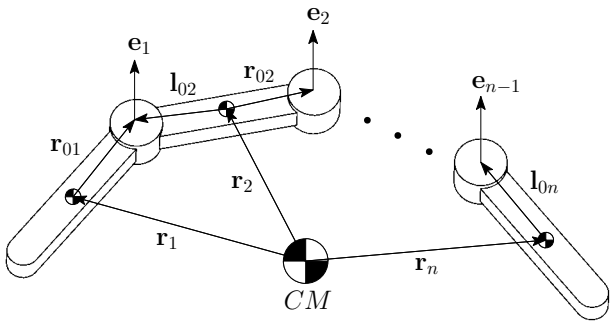

Fig. 6. Geometric modelling of the robot.

where m_i is the mass of link i. Moreover, the conservation of the angular momentum leads to

$$\frac{d\mathbf{h}}{dt} = \mathbf{0}\,, \quad \mathbf{h} = \sum_{i=1}^{n} (\mathbf{I}_i \boldsymbol{\omega}_i + m_i \mathbf{r}_i \times \mathbf{v}_i) \tag{2}$$

where $\mathbf{h}$ is the angular momentum, $\mathbf{I}_i$ is the inertia tensor of link i and $\boldsymbol{\omega}_i$ is its angular velocity. As previously stated, it is assumed that the robot is initially at rest ($\boldsymbol{\omega}_i = \mathbf{v}_i = \mathbf{0}, i = 1, \ldots, n$) and that no external torque is applied to it during the reorientation, thus $\mathbf{h}$ is set to $\mathbf{0}$.

To compute (2), each term must be expressed in the same reference frame, in this case R_0. The rotation from reference frame R_{i-1} to reference frame R_i can be expressed with matrix $\mathbf{Q}_i$. This $\mathbf{Q}_i$ matrix is defined with rotation angle θ_{i-1} about unit vector $\underline{\mathbf{e}}_{i-1}$ (expressed in its local reference frame) corresponding to the axis of the ith revolute joint. Matrix $\mathbf{Q}_1$ corresponds to the rotation from the inertial reference frame to link 1. The representation in R_0 is then obtained by pre-multiplying by the product of rotation matrices $\mathbf{Q}_1$ to $\mathbf{Q}_i$ in the case of a vector, and also by post-multiplying by the transpose of these rotation matrices in the case of a tensor.

Next, $\mathbf{r}_i$, $\mathbf{v}_i$ and $\boldsymbol{\omega}_i$ must be explicited. The derivation of these terms is based on the concept of barycentre [35], adapted to free-floating serial manipulators in [29], [15]. For each link, two constant construction vectors are defined, namely $\underline{\mathbf{r}}_{0i}$ and $\underline{\mathbf{l}}_{0i}$, as shown in Figure 6. The underscore implies that the vector or tensor is expressed in its local reference frame. Vector $\underline{\mathbf{r}}_{0i}$ connects CM_i to joint i, while vector $\underline{\mathbf{l}}_{0i}$ connects CM_i to joint $i-1$.

Combining these vectors with the mass of the links yields the position of the barycentre $\mathbf{c}_{0i}$, which is given by

$$\mathbf{c}_{0i} = \mathbf{l}_{0i}\mu_i + \mathbf{r}_{0i}(1 - \mu_{i+1}) \tag{3}$$

with μ_i the mass distribution in the robot, given by

$$\mu_i = \begin{cases} 0 & i = 1 \\ \sum_{k=1}^{i-1} \frac{m_k}{M} & i = 2, \ldots, n \\ 1 & i = n+1 \end{cases} \tag{4}$$

where M is the total mass of the robot. Vector $\mathbf{c}_{0i}$ can equivalently be found by adding a point mass $M\mu_i$ to joint $i-1$ and $M(1-\mu_{i+1})$ to joint i, which defines an augmented link [35]. The barycentre then becomes the centre of mass of

this augmented link [15]. New augmented construction vectors can be defined with respect to this centre of mass, as

$$\underline{\mathbf{c}}^*_{0i} = -\underline{\mathbf{c}}_{0i} \tag{5}$$
$$\underline{\mathbf{r}}^*_{0i} = \underline{\mathbf{r}}_{0i} - \underline{\mathbf{c}}_{0i} \tag{6}$$
$$\underline{\mathbf{l}}^*_{0i} = \underline{\mathbf{l}}_{0i} - \underline{\mathbf{c}}_{0i}. \tag{7}$$

Similarly to vector $\mathbf{r}_i$, these vectors are fully specified by the configuration of the robot, which depends on the joint angles collected in vector $\boldsymbol{\theta}$. It can be shown that $\mathbf{r}_i$ can be expressed in terms of the barycentric vectors, which yields

$$\mathbf{r}_i = \sum_{k=1}^{n} \mathbf{b}_{ki} \tag{8}$$

with $\mathbf{b}_{ki}$ defined using the following rule

$$\mathbf{b}_{ki} = \begin{cases} \mathbf{l}^*_{0k} & k > i \\ \mathbf{c}^*_{0k} & k = i \\ \mathbf{r}^*_{0k} & k < i \end{cases}. \tag{9}$$

Vector $\boldsymbol{\omega}_i$ can be expressed in R_0 by adding the angular velocity vector imparted by each joint with the angular velocity $\boldsymbol{\omega}_1$ of the first link, which yields

$$\boldsymbol{\omega}_i = \begin{cases} \boldsymbol{\omega}_1 & i = 1 \\ \boldsymbol{\omega}_{i-1} + \mathbf{e}_{i-1}\dot{\theta}_{i-1} & i = 2, \ldots, n. \end{cases} \tag{10}$$

Considering that vector $\mathbf{b}_{ki}$ is constant in the body-fixed reference frame moving with angular velocity $\boldsymbol{\omega}_i$, $\mathbf{v}_i$ is obtained as

$$\mathbf{v}_i = \sum_{k=1}^{n} \boldsymbol{\omega}_k \times \mathbf{b}_{ki} \quad i = 1, \ldots, n. \tag{11}$$

Equation (11) can be rearranged with the help of (10), yielding

$$\mathbf{v}_i = \boldsymbol{\omega}_1 \times \mathbf{r}_i + \mathbf{C}_i\dot{\boldsymbol{\theta}} \tag{12}$$

where $\mathbf{C}_i$ is a matrix of dimension $3 \times j$ which is a function of the construction parameters of the robot.

Equations (8), (10) and (12) can now be substituted into (2) — where $\mathbf{h}$ is set to zero — to form a system of equations that depends only on the unknowns $\boldsymbol{\omega}_1$ and $\dot{\boldsymbol{\theta}}$. The double vector product obtained in the process can be rearranged as

$$m_i\mathbf{r}_i \times (\boldsymbol{\omega}_1 \times \mathbf{r}_i) = m_i(\mathbf{r}_i^T\mathbf{r}_i\mathbf{1} - \mathbf{r}_i\mathbf{r}_i^T)\boldsymbol{\omega}_1 \tag{13}$$

with $\mathbf{1}$ the identity matrix.

Finally, collecting the terms in $\boldsymbol{\omega}_1$ on one side and the terms in $\dot{\boldsymbol{\theta}}$ on the other side, a linear system of equations that relates the angular velocity of the first body and the joint velocity vector of the robot is obtained as

$$\mathbf{A}\boldsymbol{\omega}_1 = \mathbf{B}\dot{\boldsymbol{\theta}} \tag{14}$$

where $\mathbf{A}$ is a 3×3 matrix and $\mathbf{B}$ is a matrix of dimension $3\times j$, which both depend on the mass of the links, the geometric parameters and the configuration of the robot. With this construction, matrix $\mathbf{A}$ is positive definite and thus invertible. This formulation of the dynamic model is general and is applicable to any spatial or planar serial free-floating robot.

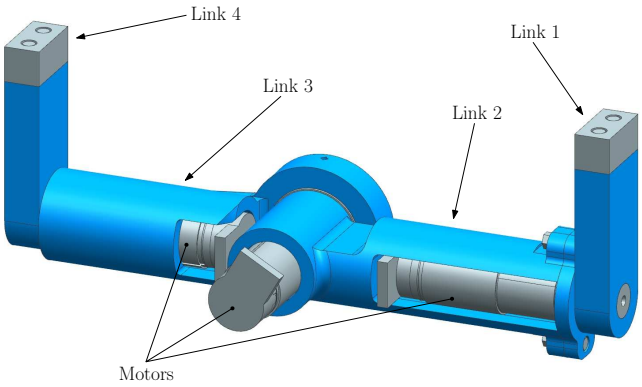

Fig. 7. CAD model of the prototype. Parts in blue are made of 3D-printed ABS plastic. Parts in grey are made of steel.

V. Prototype Design

Based on the simplified three-joint architecture presented in Section III, an experimental prototype was designed and built. A CAD model of the prototype is shown in Fig 7. The robot was designed without any on-board electronics except for the motors themselves. One drawback of this design is that it requires an experimental setup where wires must run between each motor and an external controller for power and encoder signals. The measures that were taken to mitigate the influence of the hanging wires are addressed in more details in Section VIII.

The total mass of the robot is approximately 0.3 kg. Machined steel inserts were added to the ends of links 1 and 4 in order to position their centre of mass in a way that favours the reorientation using manoeuvres A and B. The choice of an approximately symmetric architecture also favours this reorientation. Links 2 and 3 are hollow, allowing motors to be mounted inside them. The motors are 4.5 Watt brushed DC *RE-max 17* with 24:1 gearheads and 512 counts per turn encoders. The controller and command interface were implemented in *RT-Lab*. This software allows the controller to communicate with the motor drives at a rate of 1000 Hz through a QNX real-time operating system.

VI. Simulation

Using the CAD model, dynamic simulations were performed using Siemens NX to study the effects of various parameters on the dynamics of the robot in zero-gravity. Fig. 8 shows the progression of manoeuvre A simulated with the CAD model and Fig. 9 shows the progression of manoeuvre B using the same CAD model.

A. Trajectory in the joint space

The influence of the amplitudes of the movements on the net change in orientation, for manoeuvre A, was first investigated. In the joint space, this is equivalent to varying the dimensions of the rectangular loop that represents the trajectory. The final orientation as a function of maximum joint displacement is presented in Fig. 10.

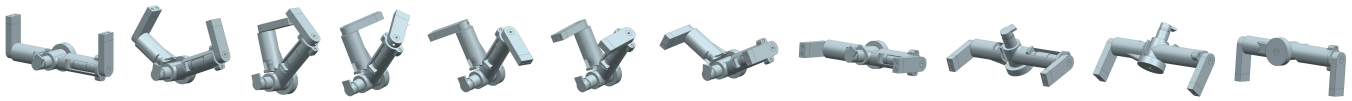

Fig. 8. Dynamic simulation of the robot executing manoeuvre A.

Fig. 9. Dynamic simulation of the robot executing manoeuvre B.

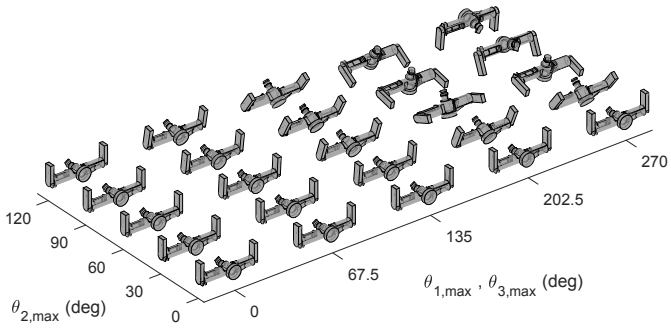

Fig. 10. Final orientation of the robot after manoeuvre A for different values of maximum joint displacement. Here, the deviation between the desired rotation matrix (pure roll rotation of $\pi/2$ angle) and the actual rotation matrix for maximum joint displacement is given by $||\mathbf{1} - \mathbf{Q}_{des}^T \mathbf{Q}_{act}||_2 = 0.0793$.

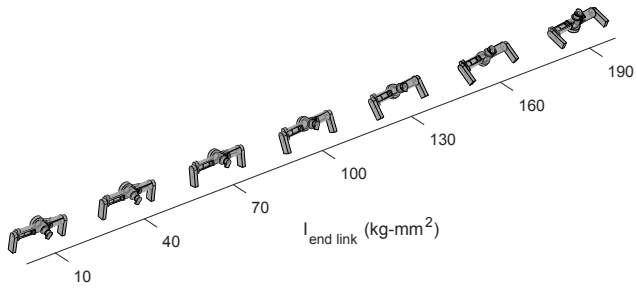

Fig. 11. Final orientation of the robot after manoeuvre A for different values of moment of inertia of the end links. All simulations are for a maximum displacement of 270 degrees at the distal joints and 120 degrees at the central joint. Here, the deviation between the desired rotation matrix (pure roll rotation of $\pi/2$ angle) and the actual rotation matrix for maximum end link inertia is given by $||\mathbf{1} - \mathbf{Q}_{des}^T \mathbf{Q}_{act}||_2 = 1.1190$. In this case, the robot "under-rotates", i.e. its roll axis rotation is less than $\pi/2$.

As it can be observed, the axis describing the net rotation induced by the manoeuvre varies very little with respect to maximum joint displacement. This means that the manoeuvre produces a rotation almost purely about the roll axis of the robot and that undesirable motions around other axes are negligible (almost nonexistent). In addition, the net rotation itself increases smoothly with respect to the maximum movement amplitude of both joints. Therefore, small internal movements of the robot produce a small reorientation while large internal movements produce a large reorientation, meaning that the manoeuvre behaves predictably. Moreover, with a reasonable displacement limit of 270 degrees for the distal joints and 120 degrees for the centre joint, a net rotation of approximately 180 degrees is predicted by the simulation. For a cat-like reorientation, a half-turn is the worst case scenario, since a rotation of more than 180 degrees is equivalent to a rotation of smaller amplitude in the opposite direction. Practically, rotating in the opposite direction can be done by reversing the direction of rotation of joints 1 and 3.

B. Moment of inertia of the end links

The effect of different inertial parameters on manoeuvre A was also studied. The starting point of this analysis is the realisation that drastically increasing the moments of inertia of links 2 and 3 results in no reorientation. Indeed, having bodies 1 and 4 linked to a very high inertia would be comparable to fixing the stators of motors 1 and 3 in space. For this reason, the study was focused on the moment of inertia of links 1 and 4 about joint axes 1 and 3, respectively. Figure 11 shows the resulting net rotation for different values of moment of inertia, with the same prescribed joint trajectories for each simulation. For this robot, it can be observed that a moment of inertia of up to approximately 100 kg-mm^2 contributes to the desired reorientation, that is, a net rotation of 180 degrees. Increasing the inertia past this point has adverse effects on the manoeuvre, notably inducing a progressively greater amount of off-axis rotation and reducing the net amount of rotation about the principal axis of the robot. Moreover, a greater moment of inertia would require higher torques at joints 1 and 3 in order to accomplish the manoeuvre.

C. Motor gear ratio and rotor inertia

With free-floating robots, extra care must be taken in the selection of the motors for joint actuation. Indeed, the motors can significantly influence the dynamic behaviour of the robot in free fall, depending on their properties. For instance, a gearmotor with a very high reduction ratio might offer more torque, but its fast spinning rotor may disturb the manoeuvre. To better characterise the influence of the gear ratio and the rotor inertia on manoeuvre A, simulations were performed with different values of these parameters. The results are shown in Fig. 12.

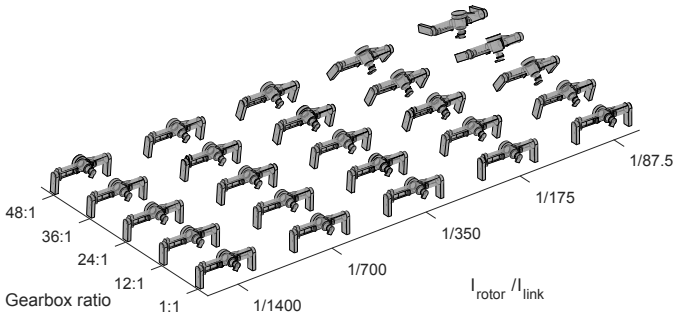

Fig. 12. Final orientation of the robot after manoeuvre A for different values of rotor inertia and gearbox ratio. All simulations are for a maximum displacement of 270 degrees at the distal joints and 120 degrees at the central joint. Here, the deviation between the desired rotation matrix (pure roll rotation of $\pi/2$ angle) and the maximum actual rotation matrix is given by $||\mathbf{1} - \mathbf{Q}_{des}^{T}\mathbf{Q}_{act}||_2 = 1.2302$. In this case, the robot "over-rotates", i.e. its roll axis rotation is more than $\pi/2$.

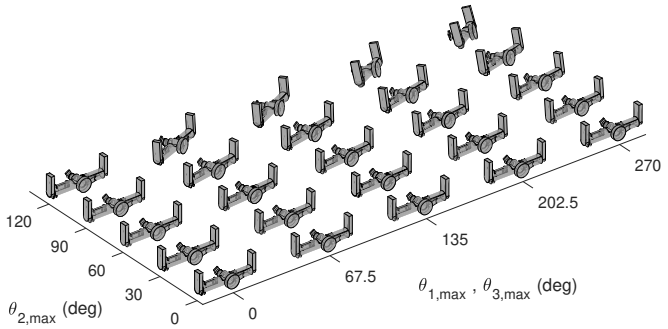

Fig. 13. Final orientation of the robot after manoeuvre B for different values of maximum joint displacement.

It can be observed that for this specific manoeuvre and geometric configuration, increasing both the moment of inertia of the rotor and the reduction ratio results in a greater net re-orientation. In other words, a smaller maximum displacement at the joints would be sufficient to achieve a net rotation of 180 degrees about the roll axis of the robot. Still, there is a trade-off between performance, form factor, weight and availability of parts, which explains the choice of a 24:1 ratio and rotor inertia of 0.1 kg-mm^2 for the current robot.

D. Simulation of Manoeuvre B

The same CAD model was used to carry out simulations for manoeuvre B. The progression of the reorientation for maximum movement amplitudes of $\theta_{1,max} = 270°$, $\theta_{2,max} = 120°$ and $\theta_{3,max} = 270°$ is shown in Fig. 9.

Fig. 13 shows the net rotation resulting from maximum movement amplitudes ranging from 0 to 270 degrees for θ_1 and θ_3 and 0 to 120 degrees for θ_2. It can be observed that for the same joint limit ranges, manoeuvre B results in a smaller net rotation than manoeuvre A. This can be attributed to the fact that the robot was designed in a way that rather favours the reorientation with manoeuvre A. Still, the robot accomplishes a maximum rotation of 43 degrees about its yaw axis, with limits of 270 degrees on joints 1 and 3 and 120 degrees on joint 2. However, off-axis rotation is also present, which means that the rotation axis is not aligned with the local axes of the robot.

Finally, similarly to manoeuvre A, there is no holonomy (no net change in orientation) when locking in position the pair of joints 1 and 3 or joint 2 ($\theta_{i,max} = 0$) while executing manoeuvre B. This is because the loop in joint space then degenerates to a line, which also corresponds to the fact that there is no change in the moment of inertia between each actuation of the remaining joint.

VII. Reaching Arbitrary Orientations

Introducing methods allowing for a specific reorientation of a robot of course naturally leads to the more general problem of arbitrary reorientation. On this subject, non-trivial results can be found in the literature. Indeed, it can be shown that any orientation can be reached with just two rotation axes, by carefully sequencing the rotations [36], [37], [38]. Most importantly, these two axes do not have to be orthogonal, which would be equivalent to any Euler angle convention where the initial axis is repeated as the last axis. However, if the axes are indeed orthogonal, any orientation can be achieved using at most 3 rotations. These conclusions can be drawn from Lowenthal's formula [36], which can be rewritten [38] as

$$N = \left\lceil \frac{\pi}{\arccos(\mathbf{m}^{\mathrm{T}}\mathbf{n})} \right\rceil + 1 \tag{15}$$

where N is the required number of alternated rotations about unit axes $\mathbf{m}$ and $\mathbf{n}$, $\arccos(\mathbf{m}^{\mathrm{T}}\mathbf{n})$ is the angle between the two axes, and $\lceil \bullet \rceil$ is the ceiling function. This equation gives an upper bound on the number of rotations needed to achieve *any* orientation, as a function of the angle between the two axes. Other methods exist [37], [38] in order to find the minimum number of rotations for a *specific* target orientation and the optimal sequence to reach it. In that case, the number of rotations needed may be lower than 3.

In the preceding sections, two distinct reorientation manoeuvres are elaborated. A cat-like manoeuvre achieves a net rotation almost purely about the longitudinal axis of the robot. The other manoeuvre allows lower amplitude rotations about a different axis. Both sequences of movements represent loops in the joint space, meaning that the robot returns to its initial configuration, but with a different orientation in space. Thus, these manoeuvres can be used as a practical implementation of this theoretical result in order to reach any orientation in space.

Lowenthal's formula and the other referenced methods are based on the assumption that an infinite rotation is possible about each axis. This may not always be the case in real life, as it is shown in this article, where specific manoeuvres coupled with joint limits produce a limited rotation. However, a large rotation about a single axis can be decomposed as a repetition of smaller rotations: the same manoeuvre can be repeated any number of times to achieve an arbitrary rotation about a single axis. Obviously, this may not be possible for terrestrial robots in free fall, since time is limited by the

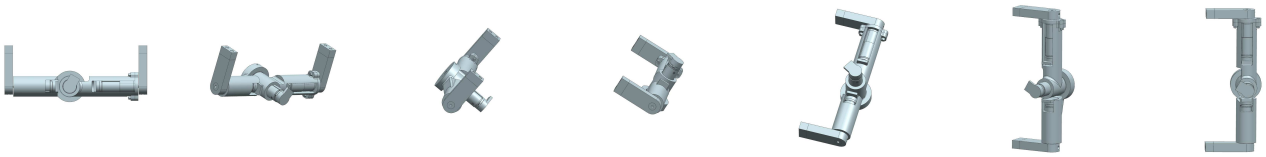

Fig. 14. Orientation of the robot at the end of each manoeuvre of the sequence. The end result is a net rotation mainly about the pitch axis of the robot, which is not directly feasible using manoeuvre A or B only.

height of the fall. Nevertheless, space robots benefit from having a virtually infinite amount of time to accomplish a sequence of manoeuvres. In that case, the movements can also be made arbitrarily slow in order to reduce the required torques at the joints to safe or allowable levels for the robot. The derivation of a mathematical framework enabling the design of such sequences of manoeuvres while considering the various constraints is out of the scope of this paper and will be the subject of future works.

Still, Fig. 14 illustrates the implications of the combination of manoeuvres. In this example, the sequence was arbitrarily chosen for demonstration purposes. To accomplish this final orientation, manoeuvres A and B are repeated or alternated a total of 6 times. The end result is a net rotation mainly about the pitch axis of the robot, which is not directly feasible using a single manoeuvre with this robot. Moreover, this orientation cannot be reached by repeating manoeuvre A or manoeuvre B alone. However, when combining them, any net rotation can be executed, even if the axes describing the net rotation induced by these manoeuvres are not orthogonal. In this example, the sequence is defined as follows:

1) Execute manoeuvre B with $\theta_{1,max} = 270°, \theta_{2,max} = 120°, \theta_{3,max} = 270°$
2) Repeat step 1
3) Execute manoeuvre A with $\theta_{1,max} = 200°, \theta_{2,max} = 80°, \theta_{3,max} = 200°$
4) Execute manoeuvre B with $\theta_{1,max} = 270°, \theta_{2,max} = 120°, \theta_{3,max} = 270°$
5) Repeat step 4
6) Execute manoeuvre A with $\theta_{1,max} = 120°, \theta_{2,max} = 120°, \theta_{3,max} = 120°$

where the sixth step only serves to compensate for the accumulated orientation error, due to the off-axis rotation induced by manoeuvre B. Numerically, the net rotation from the initial orientation of the robot to its final orientation is then

$$\mathbf{R} = \begin{bmatrix} -0.0197 & 0.0411 & -0.9990 \\ -0.1666 & 0.9858 & 0.0438 \\ 0.9858 & 0.1673 & -0.0126 \end{bmatrix} \tag{16}$$

while an ideal pure rotation of -90 degrees about the pitch axis of the robot would be given by

$$\mathbf{R}_{ideal} = \begin{bmatrix} 0 & 0 & -1 \\ 0 & 1 & 0 \\ 1 & 0 & 0 \end{bmatrix}. \tag{17}$$

The above sequence is roughly equivalent to the following ideal sequence:

1) Rotate 90 degrees about the yaw axis of the robot
2) Rotate 90 degrees about the roll axis of the robot
3) Rotate 90 degrees about the yaw axis of the robot

These results imply that, provided that enough time is allowed, a terrestrial robot could land on its legs at the end of a fall, even with a completely arbitrary starting orientation. It is also interesting to note that, although the robot presented here was not specifically designed to achieve arbitrary rotations, it is able to do so. Moreover, this robot can accomplish such arbitrary rotations using only 3 rotary actuators.

Fig. 15. Physical prototype with VICON reflective markers.

VIII. Experimental Validation

In order to validate the simulation results, the robotic prototype presented in Section V was built and an experimental set-up was designed. The prototype is shown in Fig 15.

The drop post shown in the background in Fig. 16 is a small-scale version of the typical drop towers used to simulate microgravity on Earth. The robot is not attached to the drop post during the free fall. The drop post provides 2 metres of free fall, which is equivalent to approximately 0.6 second of weightlessness. The robot lands in a flexible basket mounted on a damped spring at the end of the drop. In order to limit the influence of initial conditions as much as possible, the release mechanism consists of a set of two electromagnets. The robot is completely still before release and the manoeuvre only begins 0.02 second after the electrical current in the electromagnets is cut. This ensures that the robot is effectively free falling before it starts moving and prevents any contact with the magnets during the manoeuvre. As mentioned in Section V, the robot has no on-board electronics. To mitigate the

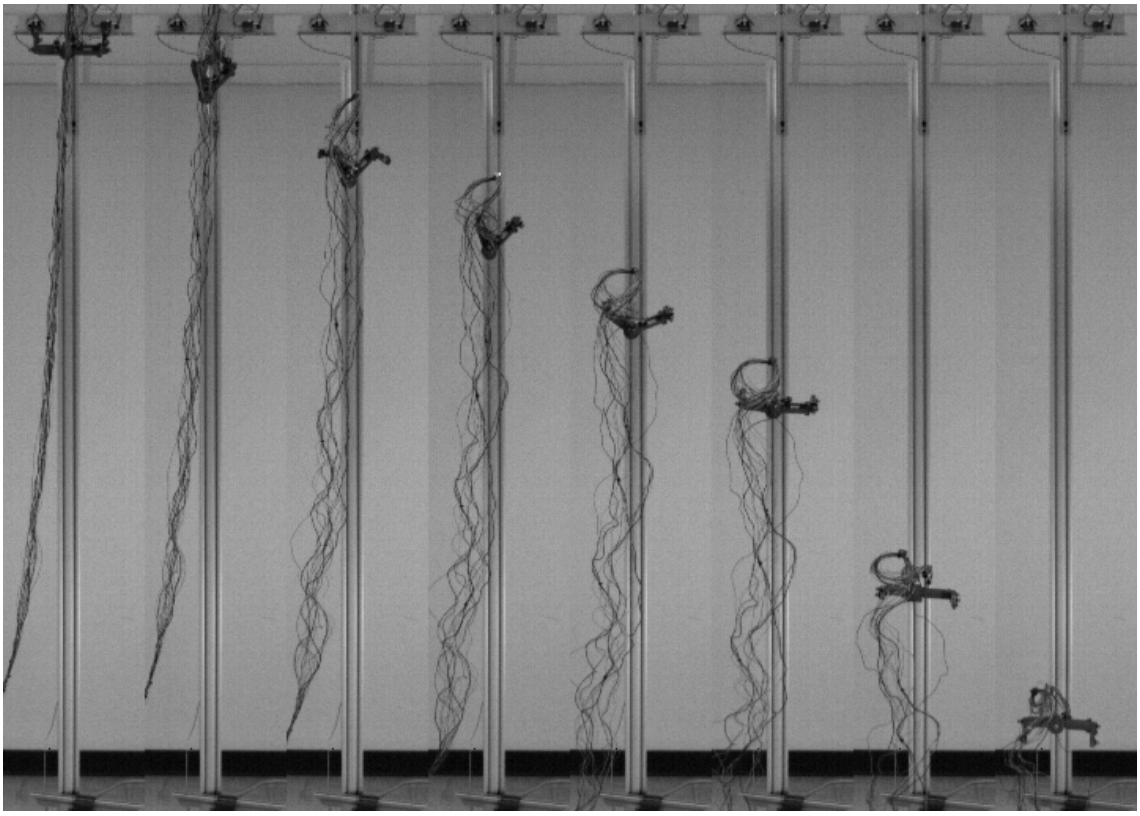

Fig. 16. Still frames from the high speed footage of the robot executing manoeuvre A.

influence of the wiring connecting the robot to the controller and power source, the thinnest possible extra flexible silicon insulated wires are used. In addition, a third electromagnet releases the wires simultaneously with the robot. This prevents the wires from pulling on the robot at the instant of release and inducing angular momentum. When the experiment is initiated, both the robot and the wires start free falling at the same time. Thus, the manoeuvre is only affected by the relatively small inertia of the wires.

For practical reasons, the drop height is limited. Thus, it is necessary to verify that the motors have enough power to execute the manoeuvre in the allowed time. To this end, the torque and speed values at each time step are extracted from the dynamic simulations of the manoeuvre and compared against the torque-speed limiting curve of the motors provided by the manufacturer. The allotted time for each step of the manoeuvre is then iteratively adjusted until a minimum-time trajectory is obtained.

It is important to note that the only control input to this robot is the relative angle between each pair of consecutive links. This means that while joints 1, 2 and 3 follow a prescribed trajectory through the use of a PID position control, the orientation of the robot in 3D space is only observed.

For qualitative analysis, the robot was filmed with a high speed camera at 800 frames per second. Fig. 16 presents still frames from a typical test drop for manoeuvre A. From these images, it can be observed that the orientation of the robot follows what was predicted by the simulations. The prototype accomplishes a half-turn net rotation at the end of the prescribed sequence of joint movements, even with the wires linked to a fixed controller.

For quantitative validation of the observations, the orientation of the first link of the robot was tracked using a VICON motion capture system at a sampling rate of 300 Hz. The markers that are required for tracking have a negligible mass and were positioned on the body so as not to hinder the manoeuvre. The motion tracker outputs the orientation of the body by fitting a given model to the measurements. Fig. 17 shows the progression of the orientation with a ZXZ Euler angle representation. It can be clearly observed that the second and third angles return to their initial value at the end of the fall, while the first angle increases by 3.35 rad. With this convention, the first angle corresponds to the roll axis of the robot. This rotation of just over 180 degrees is what was predicted by the simulation. Fig. 17 also shows that while joint coordinates did not exactly follow the prescribed curves, θ_1 and θ_3 stayed synchronised and each articulation reached the desired angular value at the prescribed time without any overlap between θ_2 and θ_1 or θ_3. Thus, the data show that the reorientation can be considered successful. Moreover, the experimentally measured orientation of link 1 closely follows the simulation results, with a RMS error of 0.24 rad on the first angle, 0.21 rad on the second angle and 0.14 rad on the third angle.

A second experiment was carried out with the same experimental set-up and motion capture system, in order to validate manoeuvre B. The results of this trial are displayed in Fig. 18. As predicted by the simulations, the final net rotation is not

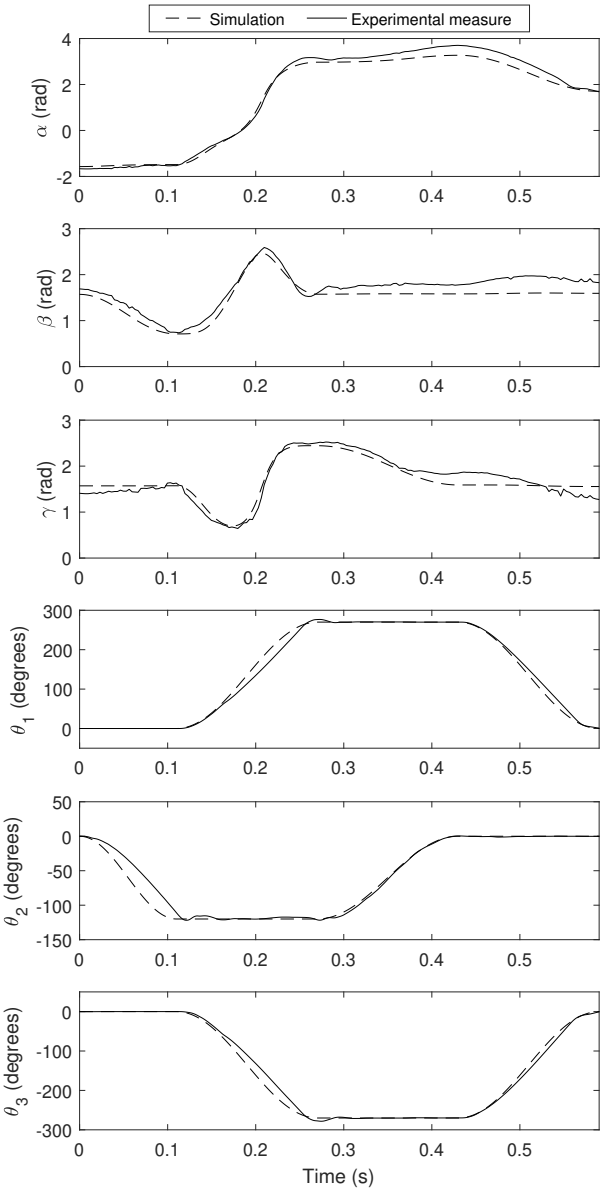

Fig. 17. Theoretical and measured (VICON motion capture) orientation of link 1 in space expressed with Euler angles α, β, γ following a ZXZ convention for manoeuvre A. Theoretical and measured joint coordinates for this manoeuvre.

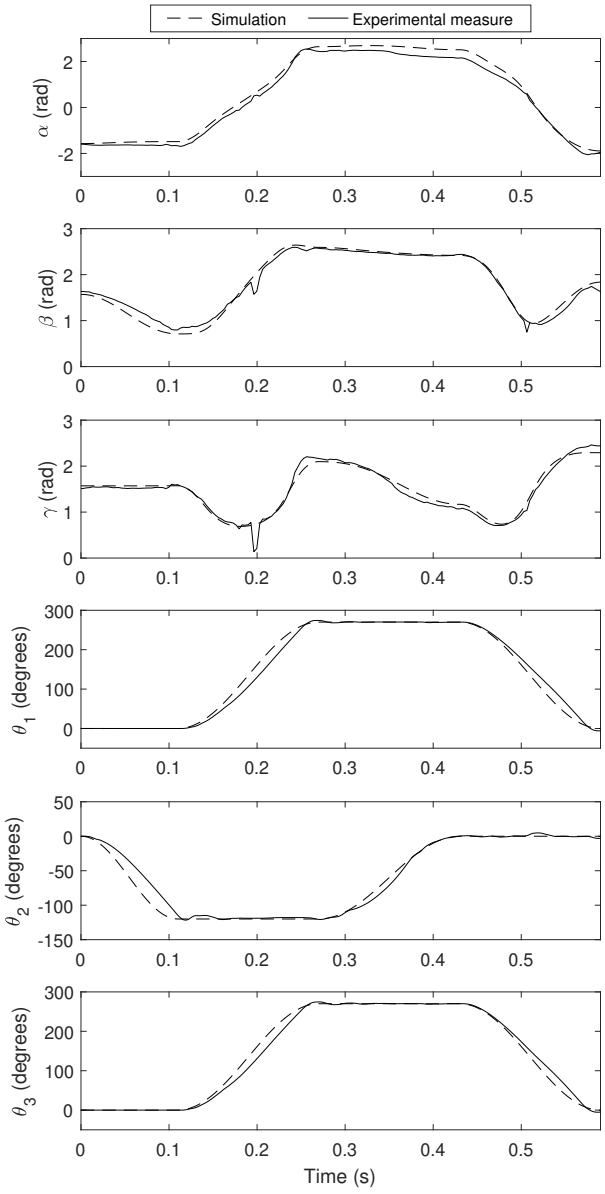

Fig. 18. Theoretical and measured (VICON motion capture) orientation of link 1 in space expressed with Euler angles α, β, γ following a ZXZ convention for manoeuvre B. Theoretical and measured joint coordinates for this manoeuvre.

purely about a single axis of the robot and thus it affects more than one of the Euler angles with the Euler angle convention used here. Still, the experimental measures tightly follow the predicted simulation values, with overall RMS errors of 0.22 rad on angle α, 0.10 rad on angle β and 0.10 rad on angle γ. The outliers that can be observed near the 0.2 second mark on angles β and γ are the result of momentarily occluded markers, leading to a wrong interpretation of the data from the VICON system. The RMS deviations are lower than those obtained with manoeuvre A, for every Euler angle. This suggests that manoeuvre B may be less prone to disturbances induced by the hanging wires, notably because the connectors on the robot point up for the whole duration of the drop, and the wires are not dragged in different directions. By contrast, the last step of manoeuvre A requires a significant movement of the wires.

To summarise, the experimental robot followed the desired joint trajectories and this in turn resulted in a measured change in orientation close to what was predicted in simulation. It is worth restating that these data serve to show that the numerical simulation is valid and that the properties exhibited by the manoeuvres can then be reproduced in real life. The results shown in this section should not be interpreted as a claim on the precision of a reorientation strategy.

IX. Conclusion

Two reorientation manoeuvres were elaborated and tested with a robotic prototype. The cat-like movement sequence achieved a net rotation of a half-turn almost purely about the roll axis of the robot. The other manoeuvre allowed a maximum rotation of 43 degrees, mainly about the yaw axis of the robot. Furthermore, the manoeuvres proved stable with respect to maximum joint displacement. That is, lowering the limits on either the central or distal joints only resulted in a smaller net rotation about the same axis. Thus, a large rotation about a single axis can be performed using a repetition of smaller rotations: the same manoeuvre can be repeated any number of times to achieve an arbitrary rotation about a single axis. Most importantly, in addition to being able to decompose large rotations about a fixed axis, arbitrary net rotations about *any* axis can be achieved by alternating the manoeuvres. Admittedly, this may not always be possible for terrestrial robots in free fall, since time is limited by the height of the fall. Nevertheless, the proposed technique can be used for space robots, where the time taken to accomplish the manoeuvre is not a limitation and where motions can be performed very slowly in order to reduce the required joint torques and ensure safety.

It is also worth restating that the presented proof of concept prototype was originally designed with the intent of validating manoeuvre A. Still, the two manoeuvres lend themselves to a typical 7-DOF shoulder-elbow-wrist serial manipulator architecture. This type of serial robot is frequent in space applications and notable examples include Canadarm2, the European Robotic Arm and the DARPA FREND arm [39]. Moreover, it should be noted that the approximately symmetric design of the prototype is not a necessary condition for the final conclusion of this work, i.e. an asymmetric robot could also reach any orientation is space with two distinct manoeuvres. Finally, terrestrial walking or jumping robots can be envisioned based on this architecture and it is interesting to note that no special or dedicated appendages were used here for reorientation.

A limitation of our study is that the proposed manoeuvres only work as intended in the absence of angular momentum. If the robot already has angular momentum, moving its links can result in off-axis spins that are more complex to predict, such as when a diver performs a twisting somersault [9]. Additionally, as the robot used in this work for the experimental validation is a proof of concept, only the motors in the joints of the robot are controlled in closed-loop. This means that the orientation of the robot in space is only controlled in open-loop. As previously stated, there are no on-board electronics, hence no sensors for feedback and reaction to disturbances. Consequently, future work will notably consist in integrating sensors providing information on the orientation of the robot. Incorporating this information in the control loop will enable the development of methods which allow the robot to react to disturbances. Moreover, the automated synthesis of sequences that rely on the two basic manoeuvres to yield arbitrary rotations (such as the sequence in Section VII) will also be the subject of future work.

Multimedia Attachment

The video included with this paper shows the graphical results of the simulation, along with clips of a typical drop test filmed with a high-speed camera.

Acknowledgment

The authors would like to thank Thierry Laliberté, Simon Foucault, Denis Ouellet and Sylvain Comtois for their help with the experiments.

References

[1] T. R. Kane and M. P. Scher, "A dynamical explanation of the falling cat phenomenon," *International Journal of Solids and Structures*, vol. 5, no. 7, pp. 663–670, 1969.

[2] A. Shapere and F. Wilczek, "Gauge kinematics of deformable bodies," *American Journal of Physics*, vol. 57, no. 6, pp. 514–518, jun 1989.

[3] E. C.-Y. Yang, P. C.-P. Chao, and C.-K. Sung, "Optimal Control of an Under-Actuated System for Landing With Desired Postures," *IEEE Transactions on Control Systems Technology*, vol. 19, no. 2, pp. 248–255, mar 2011.

[4] J. T. Bingham, J. Lee, R. N. Haksar, J. Ueda, and C. K. Liu, "Orienting in mid-air through configuration changes to achieve a rolling landing for reducing impact after a fall," in *2014 IEEE/RSJ International Conference on Intelligent Robots and Systems*. IEEE, sep 2014, pp. 3610–3617.

[5] A. Jusufi, D. T. Kawano, T. Libby, and R. J. Full, "Righting and turning in mid-air using appendage inertia: Reptile tails, analytical models and bio-inspired robots," *Bioinspir. Biomim. 5 045001 Bioinsp. Biomim*, vol. 5, pp. 45 001–12, 2010.

[6] E. Chang-Siu, T. Libby, M. Tomizuka, and R. J. Full, "A lizard-inspired active tail enables rapid maneuvers and dynamic stabilization in a terrestrial robot," in *2011 IEEE/RSJ International Conference on Intelligent Robots and Systems*. IEEE, sep 2011, pp. 1887–1894.

[7] J. Zhao, T. Zhao, N. Xi, M. W. Mutka, and L. Xiao, "MSU Tailbot: Controlling Aerial Maneuver of a Miniature-Tailed Jumping Robot," *IEEE/ASME Transactions on Mechatronics*, vol. 20, no. 6, pp. 2903–2914, dec 2015.

[8] B. Katz, J. D. Carlo, and S. Kim, "Mini Cheetah: A Platform for Pushing the Limits of Dynamic Quadruped Control," in *2019 International Conference on Robotics and Automation (ICRA)*. IEEE, may 2019, pp. 6295–6301.

[9] C. Frohlich, "Do springboard divers violate angular momentum conservation?" *American Journal of Physics*, vol. 47, no. 7, pp. 583–592, jul 1979.

[10] ——, "The Physics of Somersaulting and Twisting," *Scientific American*, vol. 242, pp. 154–165, 1980.

[11] P. V. Kulwicki, E. J. Schlei, and P. L. Vergamini, "Weightless man: Self-rotation techniques," Air Force Aerospace Medical Research Lab, Tech. Rep., 1962.

[12] P. G. Smith and T. R. Kane, "The Reorientation of a Human Being in Free Fall," 1967.

[13] T. Kane and M. Scher, "Human self-rotation by means of limb movements," *Journal of Biomechanics*, vol. 3, no. 1, pp. 39–49, jan 1970.

[14] L. A. Stirling, "Development of astronaut reorientation methods : a computational and experimental study," 2008.

[15] S. Dubowsky and E. Papadopoulos, "The kinematics, dynamics, and control of free-flying and free-floating space robotic systems," *IEEE Transactions on Robotics and Automation*, vol. 9, no. 5, pp. 531–543, 1993.

[16] K. Yoshida and Y. Umetani, "Control of Space Manipulators with Generalized Jacobian Matrix." Springer, Boston, MA, 1993, pp. 165–204.

[17] M. Reyhanoglu and N. H. McClamroch, "Planar reorientation maneuvers of space multibody systems using internal controls," *Journal of Guidance, Control, and Dynamics*, vol. 15, no. 6, pp. 1475–1480, nov 1992.

[18] I. Kolmanovsky, N. H. McClamroch, and V. T. Coppola, "New results on control of multibody systems which conserve angular momentum," *Journal of Dynamical and Control Systems*, vol. 1, no. 4, pp. 447–462, oct 1995.

[19] C. Rui, I. Kolmanovsky, and N. McClamroch, "Control problems for a multibody spacecraft via shape changes: constant nonzero angular momentum," in *Proceedings of the 1997 American Control Conference (Cat. No.97CH36041)*. IEEE, 1997, pp. 1904–1908 vol.3.

[20] ——, "Nonlinear attitude and shape control of spacecraft with articulated appendages and reaction wheels," *IEEE Transactions on Automatic Control*, vol. 45, no. 8, pp. 1455–1469, 2000.
[21] Y. Federigi, "Balancing and static walking control for a compliantly actuated quadruped exploiting system inherent elasticities," Ph.D. dissertation, Università di Pisa, nov 2017.
[22] P. Arm, R. Zenkl, P. Barton, L. Beglinger, A. Dietsche, L. Ferrazzini, E. Hampp, J. Hinder, C. Huber, D. Schaufelberger, F. Schmitt, B. Sun, B. Stolz, H. Kolvenbach, and M. Hutter, "SpaceBok: A Dynamic Legged Robot for Space Exploration," in *2019 International Conference on Robotics and Automation (ICRA)*. IEEE, may 2019, pp. 6288–6294.
[23] H. Kolvenbach, E. Hampp, P. Barton, R. Zenkl, and M. Hutter, "Towards Jumping Locomotion for Quadruped Robots on the Moon," in *IEEE/RSJ International Conference on Intelligent Robots and Systems*. IEEE, 2019, p. 7.
[24] E. Chang-Siu, T. Libby, M. Brown, R. J. Full, and M. Tomizuka, "A nonlinear feedback controller for aerial self-righting by a tailed robot," in *2013 IEEE International Conference on Robotics and Automation*. IEEE, may 2013, pp. 32–39.
[25] G. Wenger, A. De, and D. E. Koditschek, "Frontal plane stabilization and hopping with a 2DOF tail," in *2016 IEEE/RSJ International Conference on Intelligent Robots and Systems (IROS)*. IEEE, oct 2016, pp. 567–573.
[26] S. W. Heim, M. Ajallooeian, P. Eckert, M. Vespignani, and A. J. Ijspeert, "On designing an active tail for legged robots: simplifying control via decoupling of control objectives," *Industrial Robot: An International Journal*, vol. 43, no. 3, pp. 338–346, may 2016.
[27] T. Libby, A. M. Johnson, E. Chang-Siu, R. J. Full, and D. E. Koditschek, "Comparative Design, Scaling, and Control of Appendages for Inertial Reorientation," *IEEE Transactions on Robotics*, vol. 32, no. 6, pp. 1380–1398, dec 2016.
[28] S. Hadi Sadati and A. Meghdari, "Singularity-free planning for a robot cat free-fall with control delay: Role of limbs and tail," in *2017 8th International Conference on Mechanical and Aerospace Engineering (ICMAE)*. IEEE, jul 2017, pp. 215–221.
[29] J.-A. Bettez-Bouchard and C. Gosselin, "Development and experimental validation of a reorientation algorithm for a free-floating serial manipulator," in *2016 IEEE International Conference on Robotics and Automation (ICRA)*. IEEE, may 2016, pp. 2733–2738.
[30] T. W. Mather and M. Yim, "Modular configuration design for a controlled fall," in *2009 IEEE/RSJ International Conference on Intelligent Robots and Systems*. IEEE, oct 2009, pp. 5905–5910.
[31] T. Kawamura, "Understanding of Falling Cat Phenomenon and Realization by Robot," *Journal of Robotics and Mechatronics*, vol. 26, no. 6, pp. 685–690, dec 2014.
[32] J. Zhao, L. Li, and B. Feng, "Effect of swing legs on turning motion of a free-falling cat robot," in *2017 IEEE International Conference on Mechatronics and Automation (ICMA)*. IEEE, aug 2017, pp. 658–664.
[33] L. Li, J. Zhao, and Y. Xia, "Landing Posture Adjustment and Buffer Performance Analysis of a Cat Robot," in *2018 2nd IEEE Advanced Information Management,Communicates,Electronic and Automation Control Conference (IMCEC)*. IEEE, may 2018, pp. 357–363.
[34] A. D. Shapere, "Gauge mechanics of deformable bodies," Ph.D. dissertation, University of California, Santa Barbara, 1988.
[35] J. Wittenburg, *Dynamics of multibody systems*. Springer Science & Business Media, 2007.
[36] F. Lowenthal, "Uniform finite generation of the rotation group," *Rocky Mountain Journal of Mathematics*, vol. 1, no. 4, pp. 575–586, dec 1971.
[37] D. D'Alessandro, "Optimal evaluation of generalized Euler angles with applications to control," *Automatica*, vol. 40, no. 11, pp. 1997–2002, nov 2004.
[38] M. Hamada, "The minimum number of rotations about two axes for constructing an arbitrarily fixed rotation." *Royal Society open science*, vol. 1, no. 3, p. 140145, nov 2014.
[39] A. Flores-Abad, O. Ma, K. Pham, and S. Ulrich, "A review of space robotics technologies for on-orbit servicing," *Progress in Aerospace Sciences*, vol. 68, pp. 1–26, jul 2014.

Xavier Garant received the B.Eng. degree and the M.Sc. degree in Mechanical Engineering from Université Laval, Québec, Canada, in 2017 and 2019, respectively. He is currently working towards the Ph.D. degree in Mechanical Engineering at the *Laboratoire de robotique*, Department of Mechanical Engineering, Université Laval. His research revolves around robotics and dynamics, with a special interest in the modeling, design and control of complex robotic systems.

Clément Gosselin (Fellow, IEEE) received the B. Eng. degree in Mechanical Engineering from the *Université de Sherbrooke*, Québec, Canada, in 1985, and the Ph.D. degree from McGill University, Montréal, Québec, Canada in 1988. He was then a post-doctoral fellow at INRIA in Sophia-Antipolis, France in 1988–89. In 1989 he was appointed by the Department of Mechanical Engineering at *Université Laval*, Québec where he is a Full Professor since 1997. He is currently holding a Canada Research Chair in Robotics and Mechatronics since January 2001. He was a visiting researcher at the RWTH in Aachen, Germany in 1995, at the University of Victoria, Canada in 1996 and at the IRCCyN in Nantes, France in 1999.

His research interests are kinematics, dynamics and control of robotic mechanical systems with a particular emphasis on the mechanics of grasping, the kinematics and dynamics of parallel manipulators and the development of human-friendly robots. His work in the aforementioned areas has been the subject of numerous publications in international journals and conferences as well as of several patents and two books. He has been directing many research initiatives, including collaborations with several Canadian and foreign high-technology companies and he has trained more than 120 graduate students. He is an Associate Editor of the IEEE Robotics and Automation Letters and of the ASME Journal of Mechanisms and Robotics.

Dr. Gosselin received several awards including the ASME DED Mechanisms and Robotics Committee Award in 2008 and the ASME Machine Design Award in 2013. He was appointed Officer of the Order of Canada in 2010 for contributions to research in parallel mechanisms and underactuated systems. He is a fellow of the ASME, of the IEEE and of the Royal Society of Canada.